Letter

Quantum correlations and entanglement in generalized Dicke-Ising models

Santiago F. Caballero-Benitez*
Instituto de Física, LSCSC-LANMAC, Universidad Nacional Autónoma de México, Ciudad de México 04510, Mexico

(Received 20 March 2026; accepted 9 September 2026; published 18 November 2026)

Quantum systems inside high-Q cavities offer an excellent test bed for the control of emergent symmetries induced by light and their interplay with quantum matter. Recently, several developments in cavity experiments with neutral atoms and other quantum objects such as ions motivate the study of their quantum correlated properties and their entanglement to tailor and control the behavior of the system. Using the enhanced coupling between light and interacting matter, we explore the properties of emergent superradiant modes using Density Matrix Renomalization Group (DMRG) with the recently developed Light-Matter-DMRG algorithm modified for strongly interacting spin chains. We explore an experimentally viable generalization of the transverse Ising chain coupled to the cavity light where it is possible to induce multimode structures tailored by the light pumped into the system. We find that a plethora of scenarios can be explored with clear and accesible measurable signatures. This allows us to study the physics of emergent orders and strong quantum correlations with quantum spins where the local and long-range coupling can be efficiently simulated. We find that quantum spin nematic states with long-range order and magnon pairs emerge as the transitions to superradiant phases take place. Notably, we show that the cavity field allows the optimization of entanglement between spins for different light-induced modes, which can be used for quantum state engineering of quantum correlated states. Our methods can be used to model other hybrid quantum systems efficiently.

DOI: 10.1103/yzjp-fy85

Quantum scatterers inside high-Q cavities or confined in waveguides offer a unique opportunity to study how strong light-matter coupling can influence the emergence of macroscopic ordering and how quantum correlations determine the properties of the system. Recent advances in cavity systems with ultracold atoms [1] motivate to explore in other systems such as effective spins how the properties of the system can be controlled. Using the geometry of light, it is possible to induce modes that collectively scatter light in groups across the system [2–4]. These groups of quantum objects will have collective emission that can be exploited for quantum information purposes. Moreover, as light-matter interaction becomes strong inside the cavity, superradiance (SR) emerges [5,6], triggering a quantum phase transition [7] while modifying the collective properties of the scatterers due to cavity backaction. Thus, macroscopic order emerges controlled by how we pump light into the system by design. In an array of these emitters, we can have that different macroscopic orders compete similar to atomic systems where several quantum correlated states have been observed, such as insulators and supersolids [8–10], while magnetic ordering is also possible [11–13]. In effective spin systems inside cavities such as neutral atoms [14,15], Rydberg atoms [16–18], ions in waveguides [19,20] using the motional degrees of freedom, and in atoms near waveguides [21,22], the situation is similar structurally, which motivates our work. With this in mind, we study a prototypical setup to explore the collective properties of interacting spins with its interplay with cavity light in a one-dimensional setup. The interaction mediated by the cavity effective couples all the spins in the system with a global structured interaction that competes with the underlying structure that the spins have. The spins in their most simple form can interact with each other as in the Ising model, providing the system with effectively an anharmonic deformation to the energy structure of the system. The fact that now the system has many-body interactions in two fronts via the cavity light and the direct spin interactions will trigger competition of orders akin to the situation in ultracold atomic systems. As a consequence of this, quantum phase transitions emerge and the SR phases can have nontrivial properties. Further, we present a rich landscape of quantum many-body phases for the spin ordering with useful properties in the structures seeded by light for quantum information purposes as the entanglement can be controlled by design. For the simulations of the system, we employ the Light-Matter-DMRG algorithm [23] (see the Supplemental Material [24]). Recently, similar methods have been applied with the single-mode case [25] and other methods have been studied [26,27].

The model. The many-body Hamiltonian of the system rotating at frequency ω_p, following analog atomic system methods [28,29], is

$$\mathcal{H} = -\hbar\Delta_c \hat{a}^\dagger \hat{a} + \hbar\omega_0 \sum_n \hat{S}_n^z + \hbar J \sum_n \hat{S}_n^z \hat{S}_{n+1}^z + \frac{\hbar V_p}{\sqrt{N}}(\hat{a}^\dagger + \hat{a}) \sum_n J_n^{pc} \hat{S}_n^x, \tag{1}$$

*Contact author: scaballero@fisica.unam.mx

Published by the American Physical Society under the terms of the Creative Commons Attribution 4.0 International license. Further distribution of this work must maintain attribution to the author(s) and the published article's title, journal citation, and DOI.

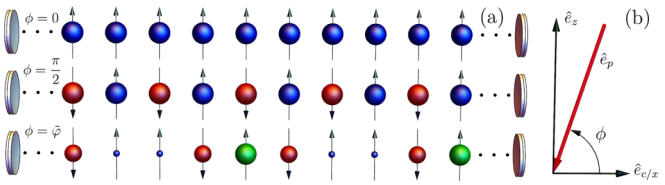


FIG. 1. Light mode structure induced to the spin chains in the cavity [panels (a) and (b)]. Experimental scheme for the light. (a) Spins along the chain; sphere size is proportional to the light mode coupling strength at each site. In the diffraction maxima configuration ($\phi = 0$), a ferromagnetic mode is induced (●●). The diffraction minima configuration ($\phi = \pi/2$) generates a staggered spin field (●●). The golden ratio (RBBRG) configuration ($\phi = \arccos(1/5) = \tilde{\varphi}$) induces a three-mode staggered spin structure (red, blue, green) every five sites [●●●●●]. The arrows point in the direction of the spin in the quantization axis "x". (b) The light setup; the angle ϕ between the cavity axis $\hat{e}_c$ and the light pumped into the system with direction $\hat{e}_p$ ($-\hat{e}_p$) for a standing wave cavity and retroreflected pump beams in the pump axis from the side (only one is shown, the other one is parallel). The light polarization unit vector is $\hat{e}_z$ and the spins are along the spatial axis $\hat{e}_x$.

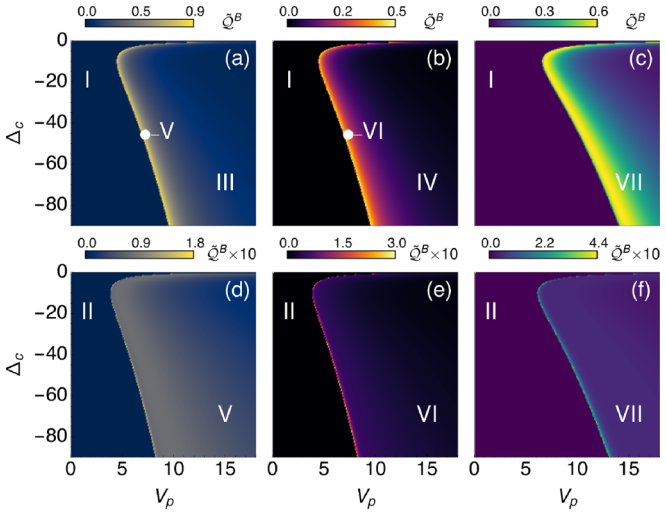


FIG. 2. Phase diagrams for different light-induced mode structures and the behavior of the mean bond nematic order parameter ($\tilde{\mathcal{Q}}^B$). When the system becomes superradiant and the quantization axis of the spins changes, there is the formation of bond nematic quantum states. These can persist deeper into the superradiant state depending on the short-range spin interaction strength J and the light-induced configuration. Panels (a)–(c) correspond to $J < 0$, normal FM state (I) and superradiant configurations (III–VII). Panels (d)–(f) correspond to $J > 0$, normal AFM state (II) and superradiant configurations (V–VII). The light-induced mode structures are given in panels (a) and (d) for $\phi = 0$ diffraction maxima (●●), in panels (b) and (e) for $\phi = \pi/2$ diffraction minima (●●), and in panels (c) and (f) for $\phi = \arccos(1/5)$, the golden ratio configuration (●●●●●), as shown in Fig. 1(a). The order parameters of different phases are provided in Table I. Parameters in the simulations are $N = 400$ spins, $\omega_0/|J| = 0.1$, and $\kappa/|J| = 10$, with Δ_c and V_p in units of $|J|$.

where the first term is the energy of the cavity photons, $\Delta_c = \omega_p - \omega_c$ is the cavity detuning, $\hbar$ is the reduced Planck constant, and $\hat{a}^{(\dagger)}$ is the cavity mode photonic annihilation (creation) operator. The energy of each spin 1/2 is $\hbar\omega_0$; the interaction between spins in the absence of cavity light is given by the Ising Hamiltonian, with $\hbar J$ the energy of the exchange of spins. The interaction between the photons and the spins is given in the typical Dicke form [1,11,30], with $\hbar V_p$ the effective pump potential; the overlap amplitudes of the spins with the pump and cavity light are given by $J_n^{pc} = \cos(\pi n)\cos(\pi n \cos\phi)$ at each localized spin with site n and N spins; the angle between the pump wave vector $\mathbf{k}_p = |\mathbf{k}_p|\hat{e}_p$ and the cavity wave vector $\mathbf{k}_c = |\mathbf{k}_c|\hat{e}_c$ is ϕ; and the spins are along $\hat{e}_x$, as shown in Fig. 1 (see the Supplemental Material [24]). Similar to atomic systems [2–4], we consider three different configurations depending on the light-induced emergent coupling of the spins due to the cavity field: For $\phi = 0$, the coupling is homogeneous across the lattice inducing a single mode; with $\phi = \pi/2$, we induce a two-mode staggered ordering with couplings $J_n^{pc} = (-1)^n$; and with $\phi = \arccos(1/5) \approx 0.436\pi$, the golden ratio mode, we induce a pattern (RBBRG) for the couplings $J_n^{pc} = \{-\varphi/2, (\varphi-1)/2, (\varphi-1)/2, -\varphi/2, 1\}$ every five sites, with $\varphi \approx 1.618\,03$ the golden ratio. The particular choice of the golden ratio mode is motivated by the fact that this configuration is the minimal case where couplings have just three different nonzero values and the structure allows for these three modes to scatter light with the same phase for each group of sites across the whole lattice. Indeed, other choices with this property with more modes at different angles can be found as we will see below. Additional choices with sets with groups of sites without coupling to the cavity light have been explored in Refs. [2–4]. To achieve a conmensurable pattern of these modes reliably, the precision in the control of the angle scales as $|\delta\phi| \gtrsim 10^{-2}/N$, for an accuracy of $S(\delta\phi) \sim 10^{-2}$ (see the Supplemental Material [24] for details).

The order parameters. In spin systems, one-body order parameters that characterize the magnetic ordering in the system are the magnetizations $\mathcal{M}_\theta^\nu = \sum_n \cos(\theta n)\langle\hat{S}_n^\nu\rangle/N$, with $\nu \in \{x, y, z\}$ and $\theta = 0$ for the magnetization, signaling Ferromagnetic (FM) ordering, or $\theta = \pi$ for the staggered magnetization, signaling Antiferromagnetic (AFM) ordering, in the spin axis ν. Considering genuine many-body spin quantum correlations, for spin 1/2 systems the traceless bond nematic tensor of rank 2 is defined as

$$\mathcal{Q}_{nm}^{\nu\eta} = \left\langle \hat{S}_n^\nu \hat{S}_m^\eta + \hat{S}_n^\eta \hat{S}_m^\nu \right\rangle (1 - \delta_{\nu\eta})(1 - \delta_{nm})/2 \qquad (2)$$

for each pair of sites nm, with $\nu, \eta \in \{x, y, z\}$. This tensor measures the quadrupolar deformations in the system between different sites as the on-site signal is trivial for spin 1/2 systems [31,32]. The bond nematic order parameter for each pair of sites nm is the largest eigenvalue of the tensor such that $\mathcal{Q}_{nm}^B = \max(\mathrm{Sp}(\mathcal{Q}_{nm}))$. It is useful to define the average over all the pairs of sites in the lattice as the global order parameter of how nematic is the state. Thus, we define the mean bond nematic order parameter as $\tilde{\mathcal{Q}}^B = \sum_{nm} \mathcal{Q}_{nm}^B/N^2$; this is shown in Fig. 2 for the different light-induced modes in Fig. 1 and different Ising couplings (FM/AFM). Due to

TABLE I. Quantum phases of the spins and their order parameters. The order parameters are the amplitude $|\langle\hat{a}\rangle|$ of the light field, the magnetization $\mathcal{M}_0^{\nu}$, staggered magnetization $\mathcal{M}_\pi^{\nu}$, the mean bond nematic order parameter $\tilde{\mathcal{Q}}^B$, the magnon pair order parameter $\tilde{\mathcal{P}}$, and the dominant spin axis $\nu = x/z$. In the normal phases (N), $|\langle\alpha\rangle| = 0$, there is no collective photon emission. The resulting phases are combinations of normal N or superradiant order R, the dominant spin axis induced by the light, and how it is transferred to the spins generating FM/ AFM in "x" or multimode FM order with golden ratio coupling φ, the bond quadrupolar order in the spins, and the emergence of magnon pairs with long-range order.

Identifier	Phase	$\lvert\langle\hat{a}\rangle\rvert$	$\mathcal{M}_0^z$	$\mathcal{M}_0^x$	$\mathcal{M}_\pi^z$	$\mathcal{M}_\pi^x$	$\tilde{\mathcal{Q}}^B$	$\tilde{\mathcal{P}}$
I	N-FM$_z$	0	$\neq 0$	0	0	0	0	0
II	N-AFM$_z$	0	0	0	$\neq 0$	0	0	0
III	SR-FM$_x$	$\neq 0$	0	$\neq 0$	0	0	≈ 0	$\neq 0$
IV	SR-AFM$_x$	$\neq 0$	$\neq 0$	0	0	$\neq 0$	≈ 0	$\neq 0$
V	SR-FM$_x$-$\mathcal{Q}^B$	$\neq 0$	0	$\neq 0$	0	0	$\neq 0$	$\neq 0$
VI	SR-AFM$_x$-$\mathcal{Q}^B$	$\neq 0$	0	0	0	$\neq 0$	$\neq 0$	$\neq 0$
VII	SR-FM$_\varphi$-$\mathcal{Q}^B$	$\neq 0$	$\neq 0$	$\neq 0$	≈ 0	≈ 0	$\neq 0$	$\neq 0$

the "x-z" symmetry of $\mathcal{H}$, the nematic order is uniaxial with $\mathcal{Q}^B_{nm} = |\mathcal{Q}^{xz}_{nm}| \neq 0$ whenever it emerges. Clearly, this is an effect that cannot be obtained by mean-field calculations, and it clarifies the underlying mechanism that triggers the quantum phase transition due to strong quantum correlations. In addition to the nematic character of the states, it is well known that magnon pair states can be supported with nematic ordering [31,33], the magnon pairs at different sites are characterized by pair amplitude $\mathcal{P}_{nm} = \langle \hat{S}^-_n \hat{S}^-_m \rangle = \langle \hat{S}^x_n \hat{S}^x_m - \hat{S}^y_n \hat{S}^y_m - i\hat{S}^x_n \hat{S}^y_m - i\hat{S}^y_n \hat{S}^x_m \rangle$, and the global magnon pair order parameter can be defined as $\tilde{\mathcal{P}} = \sum_{nm} |\mathcal{P}_{nm}|/N^2$.

Quantum phases. We find a rich set of scenarios that can be tailored depending on the geometry of the light and the short-range Ising interaction present with either FM$_z$ or AFM$_z$ character. The underlying Ising interaction determines how the correlations induced by the cavity light form. The SR phases in the system ($|\langle\hat{a}\rangle| \neq 0$) can be FM$_x$/AFM$_x$ [Figs. 2(a) and 2(d)/2(b) and 2(e)] with weak nematic character for large V_p. In contrast, fully nematic order occurs with the FM$_\varphi$ pattern induced to the system [Figs. 2(c) and 2(f)]. All the phases present are shown in Fig. 2, and Table I provides the definitions and behavior of the order parameters for each quantum phase. Further details of all relevant order parameters can be found in the Supplemental Material [24]. We find that as the cavity light emerges, the spins twist their quantization axis leading to the formation of a uniaxial quantum spin nematic [34] as the clear signature of the quantum phase transition. Moreover, the presence of these states can be stabilized beyond the transition region with the φ light-induced spin modes in both underlying short-range FM$_z$ and AFM$_z$ couplings [Figs. 2(c) and 2(f)]. The difference between SR phases with and without nematic character originates from the emergence of quantum correlations in the nematic phase. When $\tilde{\mathcal{Q}}^B = 0$, we have only dipolar order (canted magnet) as $\langle \hat{S}^x_n \rangle \neq 0$; the system has minimal quantum correlations. From our simulations, we find that the FM$_z$ Ising interactions are better for the stabilization of bond nematic order. Intuitively, this can be understood as the rigidity of the underlying FM$_z$ state is larger with respect to the twist applied to the spin quantization axis by the cavity light with respect to the AFM$_z$ state that is already minimizing the total spin in the system in the normal state. The quantum phase transitions are strongly dependent on the light and cavity parameters; modifying the cavity detuning and the pump strength, it is possible to explore how the quantum phase transitions take place in a single setup. Surprisingly, we find that all the SR states support magnon pairs with quasi-long-range order, even with a minimal display ($\tilde{\mathcal{Q}}^B \approx 0 \neq 0$) of nematic order. Further, we perform finite size analysis across the system of the quantum covariance of spin projections, which for our system are $\delta\mathcal{Q}^B_{nm} = \langle \hat{S}^x_n \hat{S}^z_m \rangle - \langle \hat{S}^x_n \rangle \langle \hat{S}^z_m \rangle$; we find that indeed our system has true long-range bond nematic order ($\delta\mathcal{Q}^B_{nm} \neq 0$) coexisting with dipolar order as $\langle \hat{S}^x_n \rangle \neq 0$ simultanously (see the Supplemental Material [24] for details of the analysis). In contrast, performing the same analysis for the magnon pair amplitude with $\delta\mathcal{P}_{nm} = \langle \hat{S}^x_n \hat{S}^x_m \rangle - \langle \hat{S}^x_n \rangle \langle \hat{S}^x_m \rangle$ reveals that the transverse spin fluctuations exhibit quasi-long-range order. Measuring the cavity light amplitude $|\langle\hat{a}\rangle|$, the magnetizations, and the spin correlations, similarly to Refs. [11,35], it is experimentally viable to reconstruct the phase diagrams of Fig. 2. In similar setups, these are routinely produced experimentally [1]. For additional details on all the observables, see the Supplemental Material [24].

Local observables and entanglement measures. Beyond one (FM$_x$) and two (AFM$_x$) cavity-induced modes, the φ setup stabilizes entirely the bond nematic state. In Fig. 3, we can see the local structure of $\mathcal{Q}^B_{nm}$ and $\mathcal{P}_{nm}$ in the middle of the chain across all the other spins for $J > 0$ [panels (a) and (c)] and $J < 0$ [panels (b) and (d)]. This illustrates the structured character of both the magnon pairing and the nematic order in the system with quasi-long-range and true long-range order, as confirmed by our quantitative analysis of the quantum correlations. These correlations present well-defined amplitude oscillations across the whole chain similar to frustrated systems [31]. As nontrivial many-body quantum correlations are present in the system, we analyze how entanglement behaves in the system using the entanglement entropy $\mathcal{S}_E = -\mathrm{Tr}[\rho_\Omega \log(\rho_\Omega)]$ considering different subsets Ω of sites in the chain (see the insets of Fig. 3). In contrast to the strength of $\mathcal{Q}^B_{nm}$, the maximum $\mathcal{S}_E$ is larger for AFM$_z$ coupling as it favors the production of singlets than for the FM$_z$, for all partitions Ω. In insets (a.1) and (b.1), we show the entanglement of each of the three modes (R, B, G) across the whole lattice induced by the φ setting, and in insets (c.1) and (d.1) the entanglement of the groups of spin singlets embedded in the mode structure. Clearly, the components that form the singlets are more entangled and the singlets themselves have high entanglement, with respect to the G mode. Indeed, this light-matter system acts like a collective entanglement gate protocol naturally and efficiently. In contrast, the entanglement across half the chain is weak, the so-called system entanglement [black lines in insets (c.1) and (d.1)]. Therefore, carefully selecting where to encode information is vital to exploit this entanglement resource. Moreover, achieving the same entanglement properties with a linear local circuit would entail $\mathcal{O}(N^2)$ operations with a prohibitive circuit depth in contrast to our $\mathcal{O}(N)$ cavity controlled scheme (see the Supplemental Material [24] for details). Indeed, the origin of the entanglement properties

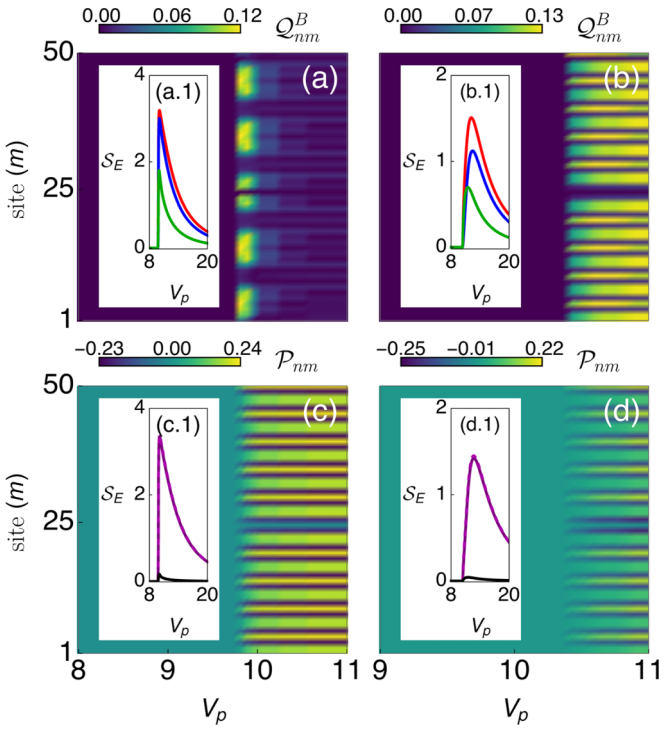


FIG. 3. Behavior with the golden ratio mode φ induced by light. Main Panels: Local bond nematic order parameter $\mathcal{Q}^B_{nm}$ and local magnon pair amplitude $\mathcal{P}_{nm}$. Insets: Entanglement entropies $\mathcal{S}_E$ for different mode structures in the system. Main panels (a) and (b) show the amplitude variation of $\mathcal{Q}^B_{nm}$ near the transition to the SR state and how long-range structured correlations emerge across the whole lattice. Main panels (c) and (d) show the amplitude variation of the magnon pairs with long-range coherent oscillations in the SR. The Ising coupling is $J > 0$ for panels (a) and (c) and $J < 0$ for panels (b) and (d). Insets (a.1) and (b.1) show the entanglement entropy of the sites with R modes (red) (● - - ● -), the B modes (blue) (- ● ● - -), and the G mode (green) (- - - - ●), across the whole lattice, following Fig. 1. Insets (c.1) and (d.1) show the entanglement entropy of the sites AFM_x singlet sites ($1+k$ and $2+k$) (solid purple, ● ● - - -) and ($3+k$ and $4+k$) (dashed purple, - - ● ● -) across the whole lattice with $k = 5 \times (n-1)$, $n = 1, \ldots, N/5$; the entanglement entropy of half the chain is shown in black. The parameters are $n = 25$ in the middle of the chain for $\mathcal{Q}^B_{nm}$ and $\mathcal{P}_{nm}$, $N = 50$ sites, $\omega_0/|J| = 0.1$, $\kappa/|J| = 10$, $\Delta_c/|J| = -50$, and V_p in units of $|J|$ for all plots.

is completely correlated with the behavior of the local spin correlations as $\mathcal{Q}^B_{nm} \equiv \langle\{\hat{S}^x_n, \hat{S}^z_m\}\rangle/2$ and the emergence of the long-range bond nematic order. Nonseparability of the quantum state originates due to $\delta\mathcal{Q}^B_{nm} \neq 0$. Whenever $\tilde{\mathcal{Q}}^B > 0$ and $\delta\bar{\mathcal{Q}}^B > 0$, we will have cavity-induced mode entanglement, which is generated efficiently by $\mathcal{O}(N)$ operations. The behavior across the transition of these light-induced modes allows for a useful qubit resource that in principle could be exploited tuning the light pumped into the system via V_p and Δ_c. Note that this is only possible due to the fact that the SR modes compete with the short-range Ising background twisting the quantization of the spins due to emergent quadrupolar coupling between different sites across the chain. In the absence of the Ising interaction or the cavity coupling, the entanglement is minimal and fragile between the spins.

In conclusion, we have found a path toward an efficient mechanism to generate highly entangled spin structures embedded in spin chains due to cavity light and its combination with short-range processes. Moreover, we have identified that this can be controlled by the geometry of light pumped into the system. It is possible to induce different concentrations of light-induced modes by choosing the angle between the cavity axis and the pumped light as $\phi = \arccos(1/(2M-1))$, with M integer; this choice will generate M modes with nonzero couplings induced by light across the system. The key ingredient to achieve this entanglement resource is the emergence of long-range bond nematic order in the system due to the anharmonic response of the spins embedded in the chain. Spin quantum correlations drive the quantum phase transition to the SR state with the emergence of magnon pairs. In principle, these magnon pairs could be used as another source to manipulate information across the chain in finite regions. We have extended our previous developments with Light-Matter-DMRG and applied the technique to analyze spin systems opening an efficient pathway toward the simulation of these light-matter systems that efficiently captures the quantum correlated nature of spin systems. Notably our work could be used for the optimization entanglement properties in the design of waveguides for analog ion systems. Our methods allow the inclusion of quantum correlated effects beyond mean-field schemes in analog qubit systems of arrays of ions [19,20], neutral atoms [14,36], Rydberg atoms [16,17], ultracold fermions [37], and possibly arrays of giant atoms [38].

Acknowledgments. We thank the hospitality of J. Hoffmann of the Physics Department of the University of Gothenburg and the Theoretical Physics Seminar where these ideas were first exposed. We thank H. Ritsch, T. Donner, F. Mivehvar, A. Frisk, and A. Bautista-Salvador for useful discussions. This work was partially supported by the grants UNAM-DGAPA-PAPIIT: IN118823, UNAM-DGPA-PAPIIT: IG101826, UNAM-CIC: Apoyo a Laboratorios Nacionales 2025, and CONAHCYT/SECIHITI: LNC-2023-51, as well as by the NVIDIA Academic Grant Program: Simulation of ultracold atomic systems via optimized methods and utilized NVIDIA RTX 6000 Ada.

Data availability. There are no publicly available research data or software supporting this manuscript. Requests for further information or data should be sent to the authors.

[1] F. Mivehvar, F. Piazza, T. Donner, and H. Ritsch, Cavity QED with quantum gases: New paradigms in many-body physics, Adv. Phys. **70**, 1 (2021).

[2] T. J. Elliott, W. Kozlowski, S. F. Caballero-Benitez, and I. B. Mekhov, Multipartite entangled spatial modes of ultracold atoms generated and controlled by quantum measurement, Phys. Rev. Lett. **114**, 113604 (2015).

[3] G. Mazzucchi, W. Kozlowski, S. F. Caballero-Benitez, T. J. Elliott, and I. B. Mekhov, Quantum measurement-induced dynamics of many-body ultracold bosonic and fermionic

systems in optical lattices, Phys. Rev. A **93**, 023632 (2016).
[4] S. F. Caballero-Benitez and I. B. Mekhov, Quantum optical lattices for emergent many-body phases of ultracold atoms, Phys. Rev. Lett. **115**, 243604 (2015).
[5] K. Baumann, C. Guerlin, F. Brennecke, and T. Esslinger, Dicke quantum phase transition with a superfluid gas in an optical cavity, Nature (London) **464**, 1301 (2010).
[6] X. Li, D. Dreon, P. Zupancic, A. Baumgärtner, A. Morales, W. Zheng, N. R. Cooper, T. Donner, and T. Esslinger, First order phase transition between two centro-symmetric superradiant crystals, Phys. Rev. Res. **3**, L012024 (2021).
[7] S. Sachdev, *Quantum Phase Transitions* (Cambridge University Press, Cambridge, 2011).
[8] R. Landig, L. Hruby, N. Dogra, M. Landini, R. Mottl, T. Donner, and T. Esslinger, Quantum phases from competing short- and long-range interactions in an optical lattice, Nature (London) **532**, 476 (2016).
[9] J. Klinder, H. Keßler, M. R. Bakhtiari, M. Thorwart, and A. Hemmerich, Observation of a superradiant Mott insulator in the Dicke-Hubbard models, Phys. Rev. Lett. **115**, 230403 (2015).
[10] J. Léonard, A. Morales, P. Zupancic, T. Esslinger, and T. Donner, Supersolid formation in a quantum gas breaking a continuous translational symmetry, Nature (London) **543**, 87 (2017).
[11] R. M. Kroeze, Y. Guo, V. D. Vaidya, J. Keeling, and B. L. Lev, Spinor self-ordering of a quantum gas in a cavity, Phys. Rev. Lett. **121**, 163601 (2018).
[12] K. Lozano-Méndez, A. H. Cásares, and S. F. Caballero-Benítez, Spin entanglement and magnetic competition via long-range interactions in spinor quantum optical lattices, Phys. Rev. Lett. **128**, 080601 (2022).
[13] B. Ríos-Sánchez and S. F. Caballero-Benítez, Control, competition and coexistence of effective magnetic orders by interactions in Bose-Einstein condensates with high-Q cavities, New J. Phys. **27**, 113203 (2025).
[14] E. Y. Song, D. Barberena, D. J. Young, E. Chaparro, A. Chu, S. Agarwal, Z. Niu, J. T. Young, A. M. Rey, and J. K. Thompson, A dissipation-induced superradiant transition in a strontium cavity-QED system, Sci. Adv. **11**, eadu5799 (2025).
[15] M. Mamaev, I. Kimchi, R. M. Nandkishore, and A. M. Rey, Tunable-spin-model generation with spin-orbit-coupled fermions in optical lattices, Phys. Rev. Res. **3**, 013178 (2021).
[16] K. A. Yasir and W.-M. Liu, *Rydberg Atoms in Cavity*, 1st ed (Springer Nature, Singapore, 2026).
[17] J. De Santis, B. Dura-Kovács, M. Öncü, A. Bouscal, D. Vasileiadis, and J. Zeiher, Realization of a cavity-coupled Rydberg array, arXiv:2602.12152.
[18] J. Gelhausen, M. Buchhold, A. Rosch, and P. Strack, Quantum-optical magnets with competing short- and long-range interactions: Rydberg-dressed spin lattice in an optical cavity, SciPost Phys. **1**, 004 (2016).
[19] R. Srinivas, S. C. Burd, R. T. Sutherland, A. C. Wilson, D. J. Wineland, D. Leibfried, D. T. C. Allcock, and D. H. Slichter, Trapped-ion spin-motion coupling with microwaves and a near-motional oscillating magnetic field gradient, Phys. Rev. Lett. **122**, 163201 (2019).
[20] G. Zarantonello, H. Hahn, J. Morgner, M. Schulte, A. Bautista-Salvador, R. F. Werner, K. Hammerer, and C. Ospelkaus, Robust and resource-efficient microwave near-field entangling $^9Be^+$ gate, Phys. Rev. Lett. **123**, 260503 (2019).
[21] W. Alvarez-Giron, P. Solano, K. Sinha, and P. Barberis-Blostein, Delay-induced spontaneous dark-state generation from two distant excited atoms, Phys. Rev. Res. **6**, 023213 (2024).
[22] P. Solano, P. Barberis-Blostein, F. K. Fatemi, L. A. Orozco, and S. L. Rolston, Super-radiance reveals infinite-range dipole interactions through a nanofiber, Nat. Commun. **8**, 1857 (2017).
[23] A. U. Ramírez-Barajas and S. F. Caballero-Benitez, Structural dynamics and strong correlations in dynamical quantum optical lattices, Phys. Rev. Lett. **135**, 120602 (2025).
[24] See Supplemental Material at http://link.aps.org/supplemental/10.1103/yzjp-fy85 for cavity light details, computational methods, finite size scaling analysis, local gate circuit, and additional details of the order parameters, which includes Refs. [39–53].
[25] J. Leibig, M. Hörmann, A. Langheld, A. Schellenberger, and K. Schmidt, Quantitative approach for the Dicke-Ising chain with an effective self-consistent matter Hamiltonian, SciPost Phys. **21**, 071 (2026).
[26] A. Langheld, M. Hörmann, and K. P. Schmidt, Quantum phase diagrams of Dicke-Ising models by a wormhole algorithm, Phys. Rev. B **112**, L161123 (2025).
[27] J. Rohn, M. Hörmann, C. Genes, and K. P. Schmidt, Ising model in a light-induced quantized transverse field, Phys. Rev. Res. **2**, 023131 (2020).
[28] C. Maschler, I. B. Mekhov, and H. Ritsch, Ultracold atoms in optical lattices generated by quantized light fields, Eur. Phys. J. D **46**, 545 (2008).
[29] S. F. Caballero-Benitez and I. B. Mekhov, Quantum properties of light scattered from structured many-body phases of ultracold atoms in quantum optical lattices, New J. Phys. **17**, 123023 (2015).
[30] A. Morales, D. Dreon, X. Li, A. Baumgärtner, P. Zupancic, T. Donner, and T. Esslinger, Two-mode Dicke model from nondegenerate polarization modes, Phys. Rev. A **100**, 013816 (2019).
[31] N. Shannon, T. Momoi, and P. Sindzingre, Nematic order in square lattice frustrated ferromagnets, Phys. Rev. Lett. **96**, 027213 (2006).
[32] S. Jiang, J. Romhányi, S. R. White, M. E. Zhitomirsky, and A. L. Chernyshev, Where is the quantum spin nematic?, Phys. Rev. Lett. **130**, 116701 (2023).
[33] A. V. Chubukov, Chiral, nematic, and dimer states in quantum spin chains, Phys. Rev. B **44**, 4693 (1991).
[34] L. Chojnacki, R. Pohle, H. Yan, Y. Akagi, and N. Shannon, Gravitational wave analogs in spin nematics and cold atoms, Phys. Rev. B **109**, L220407 (2024).
[35] F. Finger, R. Rosa-Medina, N. Reiter, P. Christodoulou, T. Donner, and T. Esslinger, Spin- and momentum-correlated atom pairs mediated by photon exchange and seeded by vacuum fluctuations, Phys. Rev. Lett. **132**, 093402 (2024).
[36] E. S. Cooper, P. Kunkel, A. Periwal, and M. Schleier-Smith, Graph states of atomic ensembles engineered by photon-mediated entanglement, Nat. Phys. **20**, 770 (2024).
[37] V. Helson, T. Zwettler, F. Mivehvar, E. Colella, K. Roux, H. Konishi, H. Ritsch, and J.-P. Brantut, Density-wave ordering in a unitary Fermi gas with photon-mediated interactions, Nature (London) **618**, 716 (2023).

[38] G. Chen and A. Frisk Kockrum, Scalable quantum simulator with an extended gate set in giant atoms, Quantum **10**, 1992 (2026).

[39] W. Kozlowski, S. F. Caballero-Benitez, and I. B. Mekhov, Probing matter-field and atom-number correlations in optical lattices by global nondestructive addressing, Phys. Rev. A **92**, 013613 (2015).

[40] S. R. White, Density matrix formulation for quantum renormalization groups, Phys. Rev. Lett. **69**, 2863 (1992).

[41] U. Schollwöck, The density-matrix renormalization group, Rev. Mod. Phys. **77**, 259 (2005).

[42] M. Fishman, S. R. White, and E. M. Stoudenmire, Codebase release 0.3 for ITensor, SciPost Phys. Codebases 4 (2022).

[43] T. Giamarchi, *Quantum Physics in One Dimension* (Oxford University Press, Oxford, 2003).

[44] F. D. M. Haldane, Luttinger liquid theory of one-dimensional quantum fluids. I. Properties of the Luttinger model and their extension to the general 1D interacting Fermi gas, J. Phys. C: Solid State Phys. **14**, 2585 (1981).

[45] A. Camacho-Guardian, R. Paredes, and S. F. Caballero-Benítez, Quantum simulation of competing orders with fermions in quantum optical lattices, Phys. Rev. A **96**, 051602(R) (2017).

[46] G. Mazzucchi, S. F. Caballero-Benitez, and I. B. Mekhov, Quantum measurement-induced antiferromagnetic order and density modulations in ultracold Fermi gases in optical lattices, Sci. Rep. **6**, 31196 (2016).

[47] S. F. Caballero-Benitez, Stability of Majorana zero modes with quantum optical lattices, New J. Phys. **28**, 103503 (2026).

[48] M. Lewenstein, A. Sanpera, and V. Ahufinger, *Ultracold Atoms in Optical Lattices: Simulating Quantum Many-Body Systems* (Oxford University Press, Oxford, 2012).

[49] J. D. Biamonte and P. J. Love, Realizing nearest-neighbor quantum circuits on one-dimensional architectures, Phys. Rev. A **78**, 012352 (2008).

[50] G. Li, Y. Ding, and Y. Xie, Tackling the qubit mapping problem for NISQ-era quantum devices, in *Proceedings of the Twenty-Fourth International Conference on Architectural Support for Programming Languages and Operating Systems (ASPLOS)* (ACM Press, Providence, RI, 2019), pp. 1001–1014.

[51] H. J. Briegel, D. E. Browne, W. Dür, R. Raussendorf, and M. Van den Nest, Measurement-based quantum computation, Nat. Phys. **5**, 19 (2009).

[52] M. Saffman, Quantum computing with neutral atoms, J. Phys. B: At. Mol. Opt. Phys. **49**, 202001 (2016).

[53] B. Nash, V. Gheorghiu, and M. Mosca, Quantum circuit optimizations for NISQ architectures, Quantum Sci. Technol. **5**, 025010 (2020).